doi: 10.15940/j.cnki.0001-5245.2024.04.011

The Correlation between Galaxy Size and Halo Mass from Galaxy-galaxy Lensing*

YAN Da-wei[1,2] WANG Qing-qing[1,2] ZHANG Cong-cong[1,2] LUO Wen-tao[1,2†]
FANG Wen-juan[1,2‡] ZHANG Yu-fei[3] LI Jia-xun[1,2]

(1 Department of Astronomy, School of Physical Sciences, University of Science and Technology of China, Hefei 230026)
(2 School of Astronomy and Space Science, University of Science and Technology of China, Nanjing 210023)
(3 College of Mathematics and Physics, Leshan Normal University, Leshan 614000)

Abstract The correlation between galaxy size and halo mass is meticulously examined through the application of galaxy-galaxy lensing techniques. The galaxy samples from Sloan Digital Sky Survey Data Release 7 (SDSS DR7) group catalog are divided into different sub-samples according to their sizes, stellar mass and color. The halo mass of each sub-sample is obtained by modeling the measured excess surface density. Blue or red galaxies do not exhibit a strong correlation between halo mass and galaxy size. The slope of the fitted halo mass to size relation for the blue and red sub-samples are $0.0237^{+0.0004}_{-0.0108}$ and $-0.0023^{+0.0002}_{-0.0054}$, respectively. The results are compared to those from the Illustris-TNG (The Next Generation Illustris project) hydrodynamic simulations, using the half-stellar mass radius provided by the database. Unlike the observations, the halo mass from simulations does show an increasing trend which mainly caused by the fact that there is positive correlation between stellar mass and galaxy size. While dividing the halo mass by the stellar mass causes this dependence to vanish, the results indicate a similarity to those obtained in this work.

Key words gravitational lensing: weak, galaxies: halos, galaxies: fundamental parameters, methods: data analysis

Classified index: P159; **Document code:** A

Received 2023-05-22, revised version 2023-06-06

*Supported by the National Key R&D Program of China Grant No. 2021YFC2203102 and 2022YFF0503404, by the National Natural Science Foundation of China Grants No. 12173036, 11773024, by the China Manned Space Project Grant No. CMS-CSST-2021-B01, by the Fundamental Research Funds for Central Universities Grants No. WK3440000004 and WK3440000005.

†wtluo@ustc.edu.cn

‡wjfang@ustc.edu.cn

1 Introduction

Most of the matter in our universe under the Λ-Cold Dark Matter (ΛCDM) cosmological model is dark matter, with observable matter only accounting for around 17%. Cold dark matter decoupled and began the formation of cosmic structures earlier than baryons. Modern galaxy formation theory suggests that galaxies form in dark matter halos, whose gravitational potential accrete gas and therefore make star formation possible. Therefore, the connection between galaxies and halos is a key issue in understanding galaxy formation and evolution. Many studies of the stellar-to-halo mass relation (SHMR) of galaxies show that massive galaxies tend to live in massive dark matter halos[1]. However, more detailed studies have found that this relation is not a simple linear or power law form[2–7], and usually have a non-negligible dispersion (about 0.2 dex[8]). The physical mechanism behind this dispersion is still unclear[9–10]. Therefore, further research on the relationship between galaxies' second-order parameters (such as galaxy size) and halo mass is crucial to deepen our understanding of SHMR.

The size of galaxies, as one of their primary observable properties, has been widely studied as a second-order parameter of SHMR. However, there is still no consensus on the correlation between galaxy size and halo mass at fixed stellar mass: some studies have shown positive correlation[8, 11–13], while others have found no significant correlation[14–20], and some even propose a negative correlation[21–24]. For instance, Charlton et al.[8] studied the correlation between galaxy size and halo mass using the galaxy-galaxy lensing technique with Canada-France-Hawaii Telescope Lensing Survey (CFHTLenS) shape catalog[25]. They found a significantly positive correlation between galaxy size and halo mass when stellar mass is controlled. Huang et al.[13] used Hyper Suprime-Cam (HSC)[26] Y1 shape catalog[27] to measure the halo mass of a massive galaxy sample with spatial resolved stellar mass data. They found that stellar-to-halo mass relation varies with different apertures, which was explained as a positive correlation between galaxy size and halo mass. Their qualitative results were consistent with the work of Charlton et al.[8].

However, unlike Charlton et al.[8] and Huang et al.[13], Sonnenfeld et al.[19] did not detect any correlation between galaxy size and halo mass at fixed stellar mass. With HSC Y1 weak lensing data and their Bayesian hierarchical approach, they investigate the correlation between galaxy observables (galaxy size, Sérsic index, and stellar mass) and weak-lensing halo mass of an early-type massive galaxy sample, which is similar to the sample utilized by Huang et al.[13].

Taylor et al.[24] used Kilo Degree Survey (KiDS)[28] shape catalog to investigate the halo mass dependence on properties of galaxies in Galaxy And Mass Assembly (GAMA). Their sample resides in a narrow range of $10.3 \leqslant \lg(M_*/M_\odot) \leqslant 10.7$ (M_* is stellar mass, $M_\odot$ is solar mass), which is the mass range near the knee of the SHMR. They concluded that within this range, there was a negative correlation between galaxy size and halo mass. But their sample consists of both star-forming and quiescent galaxies, which makes it inappropriate to directly compare their results with previous studies. With the same shape catalog, Sonnenfeld et al.[20] attempted to look for the correlation between galaxy size and halo mass of an elliptical massive central galaxy sample from the SDSS (Sloan Digital Sky Survey) DR12 spectroscopy sample. They found that, with fixed redshift and luminosity, there is no significant correlation between galaxy size and halo mass, which is consistent with their earlier result[19].

Although we have an abundance of methods to measure the mass of the dark matter halo (rotation curves, galaxy clustering, abundance matching, etc.), many of them suffer from strong modeling bias, especially some assumptions about complex baryonic processes. The galaxy-galaxy lensing technique, which exploits the shape distortions caused by the deflection of light from background galaxies as it passes through the gravitational potential of foreground lens galaxies, provides a direct and clean probe of the mass distribution of lens galaxies. It is sensitive to both baryonic and dark matter and has been widely used as a reliable method for halo mass measurements. In this work, we employ galaxy-galaxy lensing measurement to investigate the correlation between galaxy size and halo mass of a large galaxy sample from SDSS DR7. In order to maximize our sample size and thus signal-to-noise ratio, we apply a weighting method to adjust the stellar mass-redshift distribution of sample, which was presented by Luo et al.[29].

The structure of this paper is organized as follows: In Section 2, the data used in this work and the weighting method are described; the measurement of the galaxy-galaxy lensing signal and the lens model are described in Section 3 and Section 4, respectively; our main results are presented in Section 5; in Section 6, our work is discussed and analyzed; this paper is summarized in Section 7.

2 Data

2.1 SDSS DR7 galaxy shape catalog

In this work, we use the SDSS shape catalog of Luo et al.[30] based on imaging data of the SDSS Data Release 7 as the background source galaxy sample. Similar to Mandelbaum et al.[31], they only selected galaxies with OBJC_TYPE = 3 (the object is classified as an extended source ("galaxy")) from the Photometry pipeline developed by Lupton et al.[32], and required that these galaxies have apparent magnitudes brighter than 22 mag in the r band and brighter than 21.6 mag in the i band. Furthermore, they excluded the images located on the Charge-Coupled Device (CCD) boundary, affected by cosmic rays, and pixels being saturated. They applied Bernstein et al.'s technique to re-construct the point spread function (PSF)[33]. They measured the shapes of these galaxies in r band after correcting the PSF using their image processing pipeline. The shape catalog passes several regular tests and is suitable for scientific purposes. Finally, a shape catalog with coordinates, photometric redshifts, and shape measurements of 41631361 background galaxies was obtained.

2.2 Lens galaxy sample

Our lens galaxy sample is based on the SDSS DR7 group catalog of Yang et al.[34]. This group catalog is constructed from the New York University Value-Added Galaxy Catalog (NYU-VAGC)[35]. In the group catalog, all galaxies are extinction-corrected and brighter than 17.72 mag in r band, with a redshift range of $[0.01, 0.2]$. It has a wide sky coverage of 7748 square degrees. In this work, we use model C set of the group catalog (see Yang et al.[34]), which is based on c-model magnitude of SDSS. We only select galaxies with redshift range $0.02 \leqslant z \leqslant 0.2$, mass range $8 \leqslant \lg[M_*/(M_\odot \cdot h^{-2})] \leqslant 12$ (h is the reduced Hubble constant) and R_{90} (Petrosian radius, including 90% of the flux) greater than 17 kpc, and get a sample of 519891 galaxies. We obtain RA (Right Ascension), Dec (Declination), R_{90}, stellar mass $\lg[M_*/(M_\odot \cdot h^{-2})]$, spectroscopic redshift z, r band magnitude $M_{\rm r}$ (k-corrected to 0.1), and color g-r (k-corrected to 0.1) from the group catalog and NYU-VAGC.

It is well known that there is a bimodality

in the color-magnitude distribution, or M_*-SFR distribution, of galaxies[36]. Red galaxies are often early-type and their size growth is dominated by merging, while blue galaxies are more likely to be late-type and their size growth is dominated by star formation. Previous galaxy-galaxy lensing works[37] show that this bimodality also affects halo mass, where red galaxies reside in more massive dark matter halo than blue galaxies at fixed stellar mass. To control the effects of galaxy color on both galaxy size and halo mass, we divided the galaxy sample into two samples: red and blue galaxies, following the work of Yang et al.[38]. We use the following curve to separate red and blue galaxies:

$$^{0.1}(\mathrm{g}-\mathrm{r}) = 1.022 - 0.0652x - 0.0031x^2\,, \quad (1)$$

where $x = {}^{0.1}M_\mathrm{r} - 5\lg h + 23.0$. The distribution of lens galaxies in the color-absolute magnitude diagram is shown in Fig. 1, where the black curve represents Eq. (1). The galaxies above this curve are defined as red galaxies, while those below the curve are blue galaxies. We further divide the galaxies into four R_{90} bins for red and blue samples, respectively. Table 1 shows the R_{90} range, mean size $\langle R_{90}\rangle$, mean stellar mass $\langle \lg M_*\rangle$, mean redshift $\langle z\rangle$, central galaxy ratio ($N_\mathrm{cen}/N_\mathrm{sub-sample}$, N_cen is the number of central galaxies), and number of galaxies ($N_\mathrm{sub-sample}$) for the eight bins. We adjust the R_{90} range to ensure that each sub-sample has enough galaxies for a high signal-to-noise ratio of the galaxy-galaxy lensing signal. Instead of using the half-light radius, we choose the galaxy size parameter R_{90}, which is a more suitable parameter for extended light sources such as galaxies (Further discussion is provided in Section 5.2).

2.3 Weight calculation for lens sub-samples

Figure 2 is the stellar mass-redshift distribution of the first sub-sample of the red galaxies, blue galaxies and the blue galaxies after being weighted. Given that the lens galaxy sub-samples do not have the same distribution in stellar mass and redshift (see Fig. 2 (a) and Fig. 2 (b)), we add weights to each sub-sample to ensure they all have similar stellar mass-redshift distributions. The entire stellar mass-redshift distribution is divided into 21×21 bins, with the redshift and stellar mass ranges of $0.02 \leqslant z \leqslant 0.2$ and $8 \leqslant \lg[M_*/(M_\odot\cdot h^{-2})] \leqslant 12$, respectively. Finally, we use the stellar mass-redshift distribution of one sub-sample as the reference and multiply each bin of the stellar mass-redshift distribution map of other sub-samples by a weight:

$$w_\mathrm{l} = \frac{N_\mathrm{standard}(z, M_*)}{N_\mathrm{change}(z, M_*)}\,, \quad (2)$$

N_standard is the number of galaxies in the bin used as the reference, while N_change represents the number of galaxies in the bin that require add weights. Finally, our results can be seen in Fig. 2 (c). By adding weights in this way, we can make the sub-samples have nearly identical stellar mass-redshift distributions.

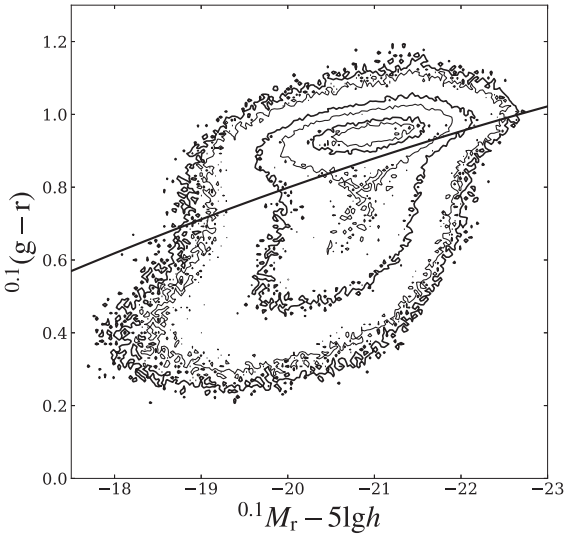

Fig. 1 The distribution of lens galaxies in color-absolute magnitude plane

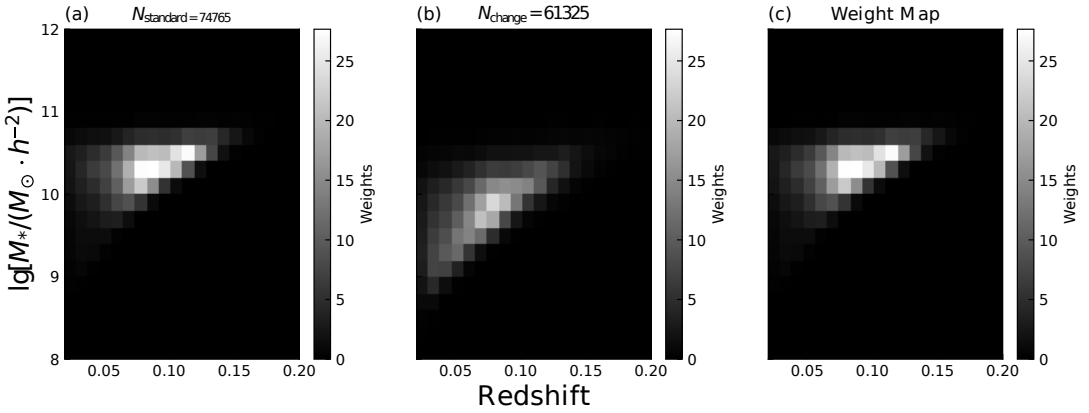

Fig. 2 (a) The stellar mass-redshift distribution of the first sub-sample of the red galaxies is used as the reference. (b) The stellar mass-redshift distribution of the first sub-sample of the blue galaxies. (c) The stellar mass-redshift distribution of the first sub-sample of the blue galaxies after being weighted. The maximum value of $w_{\rm l}$ is 27.65 and the minimum value is 0. The adding weights of other sub-samples are treated similarly.

Table 1 The parameters distribution of the eight sub-samples of red and blue galaxies

Color	R_{90} /kpc	$\langle R_{90}\rangle$ /kpc	$\langle \lg M_*\rangle$ $/(M_\odot \cdot h^{-2})$	$\langle z\rangle$	$N_{\rm cen}/N_{\rm sub-sample}$	$N_{\rm sub-sample}$
Red	17 – 24	20.53	10.33	0.083	0.65	74765
	24 – 31	27.40	10.55	0.103	0.72	69791
	31 – 41	35.61	10.73	0.123	0.77	73459
	41 – 315	54.12	10.98	0.146	0.84	75098
Blue	17 – 24	20.63	9.86	0.074	0.71	61325
	24 – 31	27.41	10.15	0.095	0.71	62805
	31 – 41	35.46	10.40	0.117	0.71	61196
	41 – 315	50.11	10.66	0.141	0.71	41452

3 Excess Surface Density (ESD) estimator

Background galaxies are affected by the weak gravitational lensing effect of foreground galaxies, which changes their shape. In galaxy-galaxy lensing, we use the angular-averaged tangential shear $\gamma_{\rm t}$ as the statistic. It is related to Excess Surface Density (hereafter ESD) as:

$$\gamma_{\rm t}(R) = \frac{\Delta\Sigma(R)}{\Sigma_{\rm cirt}}\,, \tag{3}$$

where $\Delta\Sigma(R)$ is ESD, $\Sigma_{\rm cirt}$ is critical density and R is project radius. ESD is determined by the differential profile of the projected mass density:

$$\Delta\Sigma(R) = \Sigma(\leqslant R) - \Sigma(R)\,, \tag{4}$$

where $\Sigma(R)$ denotes the average surface density at given project radius R, while $\Sigma(\leqslant R)$ represents the average surface density inside radius R. The critical density $\Sigma_{\rm crit}$ is a geometry factor:

$$\Sigma_{\rm crit} \equiv \frac{c^2}{4\pi G}\frac{D_{\rm S}}{D_{\rm LS}D_{\rm L}(1+z_{\rm l})^2}\,, \tag{5}$$

where c is speed of light in vaccum, G is Newton gravitational constant. $D_{\rm L}$, $D_{\rm S}$, and $D_{\rm LS}$ denote the angular diameter distance of lens, source, and from lens to source, $z_{\rm l}$ is the redshift of lens galaxy. We use comoving scale throughout the measurement, so the $(1+z_{\rm l})^2$ factor is necessary.

In order to achieve a high signal-to-noise ratio, it is necessary to stack the signal of background galaxies[39], so we use the following estimator to measure tangential shear and thus ESD:

$$\Delta\Sigma(R)=\frac{1}{2\mathcal{R}}\frac{\sum_l^{N_{\rm l}} w_{\rm l}\sum_s^{N_{\rm s}} e_{\rm t}\Sigma_{\rm crit}(z_{\rm l},z_{\rm s})\frac{\Sigma_{\rm crit}^{-2}(z_{\rm l},z_{\rm s})}{\sigma_{\rm e}^2+\sigma_{\rm rms}^2}}{\sum_l^{N_{\rm l}} w_{\rm l}\sum_s^{N_{\rm s}}\frac{\Sigma_{\rm crit}^{-2}(z_{\rm l},z_{\rm s})}{\sigma_{\rm e}^2+\sigma_{\rm rms}^2}}\,, \tag{6}$$

here $\mathcal{R}$ is the mean shear responsivity of our shape catalog, the variables $\sigma_{\rm e}$ and $\sigma_{\rm rms}$ refer to the shape noise and shape measurement error, respectively. $N_{\rm l}$ and $N_{\rm s}$ correspond to the number of stacked lens galaxies and source galaxies, respectively. $e_{\rm t}$ denotes the tangential ellipticity of a source galaxy residing at a projected distance of R from a lens galaxy. $z_{\rm s}$ is the redshift of source galaxy. It can be formulated as follows:

$$\mathcal{R}=1-\frac{1}{N_{\rm s}}\sum_{s=1}^{N_{\rm s}}(e_1^{\rm rot})^2\,, \tag{7}$$

where $e_1^{\rm rot}$ is the ellipticity of background galaxies after SPA (sky position angle) rotation. We divide the projected radius into 8 equal logarithmic bins from 0.01 $h^{-1}\cdot$ Mpc to 1.5 $h^{-1}\cdot$ Mpc while measuring lensing signals.

4 Model

In order to extract physical information from the galaxy-galaxy lensing signal, a lens model which describes the matter distribution around lens galaxies is crucial. In this work, we use the model proposed by Yang et al.[40] and Mandelbaum et al.[41] to fit our lensing signals. In this model ESD has four contributions: the contribution of stellar mass on small scales $\Delta\Sigma_*(R)$, the one halo term of central galaxies $\Delta\Sigma_{\rm cen}(R)$, the contribution of satellites' host halo $\Delta\Sigma_{\rm sat}(R)$, and the two halo term $\Delta\Sigma_{\rm 2halo}(R)$:

$$\begin{aligned}\Delta\Sigma(R)=\Delta\Sigma_*(R)+(1-f_{\rm sat})\Delta\Sigma_{\rm cen}(R)+\\ f_{\rm sat}\Delta\Sigma_{\rm sat}(R)+\Delta\Sigma_{\rm 2halo}(R)\,,\end{aligned} \tag{8}$$

where $f_{\rm sat}$ is the satellite fraction.

Since the galaxy size is much smaller than our measurement scales, we treat it as a point source and use the average mass of the entire lens galaxy sample to calculate ESD:

$$\Delta\Sigma_*(R)=10^{\langle\lg M_*\rangle}/\pi R^2\,, \tag{9}$$

where $\langle\lg M_*\rangle$ is the average stellar mass.

For central galaxies, we use Navarro-Frenk-White (NFW)[42] model to describe their density profile as radius r:

$$\rho(r)=\frac{\rho_0}{(r/r_{\rm s})(1+r/r_{\rm s})^2}\,, \tag{10}$$

with $\rho_0=\frac{\bar{\rho}\Delta_{\rm vir}}{3I}$, where $\bar{\rho}$ is the mean density of the universe, $\Delta_{\rm vir}=200$, $I=\frac{1}{c_{\rm c}^3}\int_0^{c_{\rm c}}\frac{x{\rm d}x}{(1+x)^2}$. The concentration parameter $c_{\rm c}=r_{\rm vir}/r_{\rm s}$ represents the ratio of a halo's virial radius $r_{\rm vir}$ and its characteristic scale radius $r_{\rm s}$.

Then, the analytical expression for the projected surface density can be derived[40]:

$$\Delta\Sigma_{\rm cen}(R)=\Delta\Sigma_{\rm NFW}(R)=\frac{M_{\rm h}}{2\pi r_{\rm s}^2 I}[g(x)-f(x)]\,, \tag{11}$$

where $x=r/r_s$ and $M_{\rm h}$ is the halo mass, the functions $f(x)$ and $g(x)$ are defined as:

$$f(x)=\begin{cases}\dfrac{1}{x^2-1}\left(1-\dfrac{\ln\frac{1+\sqrt{1-x^2}}{x}}{\sqrt{1-x^2}}\right)\,, & x<1\,,\\ \dfrac{1}{3}\,, & x=1\,,\\ \dfrac{1}{x^2-1}\left(1-\dfrac{\tan^{-1}(\sqrt{x^2-1})}{\sqrt{x^2-1}}\right)\,, & x>1\,,\end{cases} \tag{12}$$

and

$$g(x)=\begin{cases}\dfrac{1}{x^2}\left[\ln(x/2)+\dfrac{\ln\frac{1+\sqrt{1-x^2}}{x}}{\sqrt{1-x^2}}\right], & x<1\,,\\ 2+2\ln\left(\dfrac{1}{2}\right), & x=1\,,\\ \dfrac{1}{x^2}\left[\ln(x/2)+\dfrac{\tan^{-1}(\sqrt{x^2-1})}{\sqrt{x^2-1}}\right], & x>1\,.\end{cases} \tag{13}$$

The contribution of satellite galaxies comes mainly from their host halo, which can be treated as an off-centered NFW halo with an off-center distance $R_{\rm off}$. The projected surface density of an off-centered NFW halo can be expressed as:

$$\Sigma_{\rm off}(R|M_{\rm host},R_{\rm off})=\frac{1}{2\pi}\int_0^{2\pi}\Sigma_{\rm NFW}\left(M_{\rm host},\sqrt{R^2+R_{\rm off}^2+2R_{\rm off}R\cos\theta}\right)\mathrm{d}\theta. \tag{14}$$

$M_{\rm host}$ is the host halo mass. θ represents the polar angle. The next step is to parameterize $P(R_{\rm off}|M_{\rm h})$ and $P(M_{\rm host}|M_{\rm h})$, then integrate Eq. (14) over them:

$$\Sigma_{\rm sat}(R|M_{\rm h})=\int\mathrm{d}M_{\rm host}P(M_{\rm host}|M_{\rm h})\int\mathrm{d}R_{\rm off}P(R_{\rm off}|M_{\rm h})\Sigma_{\rm off}(R|M_{\rm host},R_{\rm off})\,, \tag{15}$$

where $P(R_{\rm off}|M_{\rm h})$ is the satellite spatial distribution function and $P(M_{\rm host}|M_{\rm h})$ is the host halo mass function. For satellite spatial distribution function $P(R_{\rm off}|M_{\rm h})$, we assume that the distribution of satellite galaxies follows the same NFW density profile as dark matter halos (for details, see Leauthaud et al.[43]). Following Guzik & Seljak[44], we use the product of halo mass function $n(M_{\rm h})$[45] and halo occupation distribution (HOD) function of satellite galaxies $\langle N_{\rm sat}\rangle(M_{\rm h})$ to describe host halo mass function $P(M_{\rm host}|M_{\rm h})$. Thus the projected surface density is given by:

$$\Sigma_{\rm sat}(R)=\frac{1}{C}\int_0^\infty n(M_{\rm h})\langle N_{\rm sat}\rangle(M_{\rm h})\int\mathrm{d}R_{\rm off}P(R_{\rm off}|M_{\rm h})\Sigma_{\rm off}(R|R_{\rm off},M_{\rm h})\mathrm{d}M_{\rm h}\,, \tag{16}$$

where $C=\int_0^\infty n(M_{\rm h})\langle N_{\rm sat}\rangle\mathrm{d}M_{\rm h}$ is the normalization factor. Here for $n(M_{\rm h})$, we use the halo mass function of Tinker et al.[45]. The satellite HOD function is

$$\langle N_{\rm sat}\rangle(M_{\rm h})=\Theta^H(M_{\rm h}-M_{\rm min})\left(\frac{M_{\rm h}-M_{\rm min}}{M'}\right)^\alpha. \tag{17}$$

Here, Θ^H is the Heaviside step function. Similar to Mandelbaum et al.[31], we set $\alpha=1$ and $M_{\rm min}=3M_{\rm cen}$ ($M_{\rm cen}$ is the central halo mass). However, it should be noted that Mandelbaum et al.[31] fixed the satellite fraction to be 0.2, while we treat the satellite fraction as a free parameter. M' is the amplitude of the satellite galaxy HOD function and we fixed it as a constant, as the shape of the function is only important after normalization in Eq. (16).

For the two halo term, we first generate power spectra at the mean redshift of each sample using the software pyCamb[46], then we transform power spectra into correlation functions[30]. We also employ the bias model proposed by Tinker et al.[47]:

$$\xi_{hm}=\langle b_{\rm h}\rangle\eta\xi_{mm}\,, \tag{18}$$

where ξ_{hm} is halo-matter correlation function, $\langle b_{\rm h}\rangle$ is halo bias term, ξ_{mm} is matter-matter correlation functions and

$$\eta(r)=\frac{[1+1.17\xi_{mm}(r)]^{1.49}}{[1+0.69\xi_{mm}(r)]^{2.09}}\,. \tag{19}$$

The halo bias term $\langle b_{\rm h}\rangle$ is the effective bias[31], which can be expressed as

$$\langle b_{\rm h}\rangle=(1.0-f_{\rm sat})b_{\rm h}(M_{\rm cen})+$$

$$f_{\rm sat}\int_0^{\infty} n(M_{\rm h})\langle N_{\rm sat}\rangle(M_{\rm h})b_{\rm h}(M_{\rm h}){\rm d}M_{\rm h}\,. \tag{20}$$

Then we can calculate ESD of the two halo term:

$$\Delta\Sigma_{\rm 2halo}(R)=\Sigma_{\rm 2halo}(\leqslant R)-\Sigma_{\rm 2halo}(R)\,, \tag{21}$$

where $\Sigma_{\rm 2halo}(\leqslant R)$ represents the projected surface density of the two halo term up to a radius R, while $\Sigma_{\rm 2halo}(R)$ denotes the projected surface density of the two halo term at the radius R, then

$$\Sigma_{\rm 2halo}(\leqslant R)= \frac{4\overline{\rho}}{R^2}\int_0^R x{\rm d}x\int_x^{\infty}[1+\langle b_{\rm h}\rangle\xi_{mm}(r)]\frac{r{\rm d}r}{\sqrt{r^2-x^2}}\,, \tag{22}$$

and

$$\Sigma_{\rm 2halo}(R)=2\overline{\rho}\int_R^{\infty}[1+\langle b_{\rm h}\rangle\xi_{mm}(r)]\frac{r{\rm d}r}{\sqrt{r^2-R^2}}\,. \tag{23}$$

Finally, we build the likelihood function and use the Python package emcee to run MCMC (Monte Carlo Markov Chain) to estimate the posterior distribution. We assume a Gaussian form for the likelihood function[48]:

$$\ln\mathcal{L}=-0.5[(\boldsymbol{A}-\boldsymbol{B}_{\rm model})^{\rm T}(\boldsymbol{C}^{-1}(\boldsymbol{A}-\boldsymbol{B}_{\rm model})]\,, \tag{24}$$

where $\boldsymbol{A}$ is ESD data vector, $\boldsymbol{B}_{\rm model}$ is the model prediction, and $\boldsymbol{C}^{-1}$ is the inverse of covariance matrix.

5 Result

In this section, we use galaxy-galaxy lensing to quantify the excess surface density signal and halo mass of red/blue galaxy sub-samples to investigate the correlation between galaxy size and halo mass. ESD signal is decomposed into different components using the model discussed in Section 4: stellar mass component, NFW central galaxy component, satellite galaxy component, and two halo term. The total ESD signal, along with the contributions from each component, is displayed in Fig. 3. Additionally, the corner plot illustrates the MCMC posterior distribution of the three parameters for the galaxy sub-sample. The stellar mass component (dash-dotted curve) only contributes on small scales while decreases rapidly as the scale increases. The NFW central galaxy component is usually the dominant component (dotted curve). The satellite galaxy component only has a significant contribution within the virial radius (dashed curve), and the two halo term only contributes on large scales (solid curve).

5.1 Stellar-to-halo mass relation

We take different sub-samples of the red galaxies in Table 1 as the reference, and add weights (as shown in Eq. (2)) to the blue galaxy sub-samples within the same R_{90} range. The weights can ensure the red and blue galaxy sub-samples in the same R_{90} range with same stellar mass-redshift distribution. Table 2 shows the averages of stellar mass, galaxy size $\langle R_{90}\rangle$, redshift, and the number of galaxies for each blue galaxy sub-sample after being weighted. The ESDs of each galaxy sub-sample are displayed in Fig. 4. Notably, there are subtle differences in parameters between blue and red galaxy sub-samples, and error of ESD in Fig. 4 (c) is larger than that in Fig. 4 (a) and Fig. 4 (b). This may be due to the lack of a sufficient number of galaxies in some certain bins on the stellar mass-redshift distribution map.

The correlation between stellar mass and halo mass in Table 1 is represented with solid squares and solid circles, and that in Table 2 with hollow circles, in Fig. 5. Additionally, the fitting curves for the correlation between stellar mass and halo mass derived from previous studies are also presented in

Fig. 5. We find that our stellar-to-halo mass relation is aligned with previous studies[4–6, 38], demonstrating the reliability of our weighting method. And once again, Fig. 5 proves that blue galaxies live in less massive halos compared to red galaxies of the same stellar mass[37, 49].

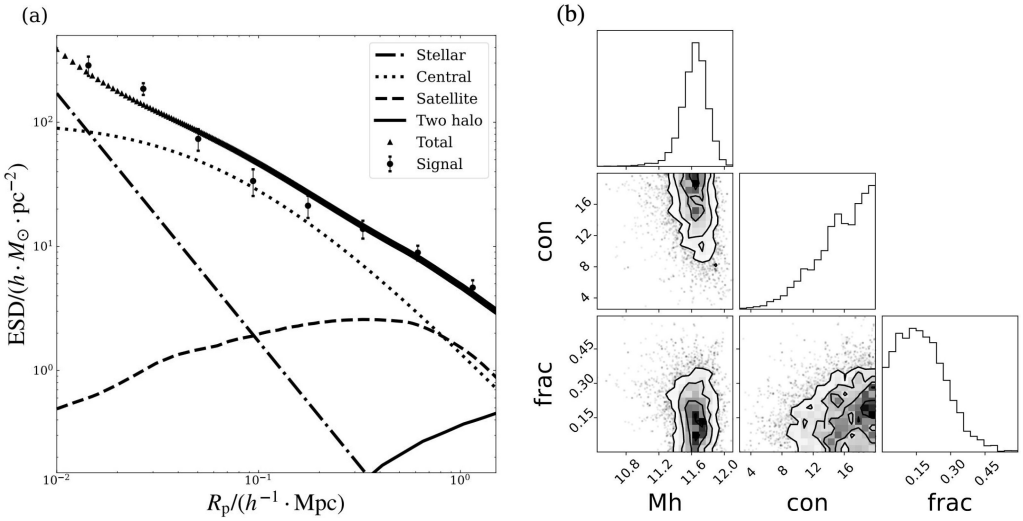

Fig. 3 (a) The total excess surface density (ESD) signal and the contributions from each component: stellar mass component (dash-dotted curve), NFW central galaxy component (dotted curve), satellite galaxy component (dashed curve), and two halo term (solid curve). $R_{\rm p}$ is the projected radius. (b) The corner plot of the three parameters in the MCMC posterior distribution of the galaxy sub-sample. Mh is the halo mass $M_{\rm h}$, con is the $c_{\rm c}$ and frac is the $f_{\rm sat}$.

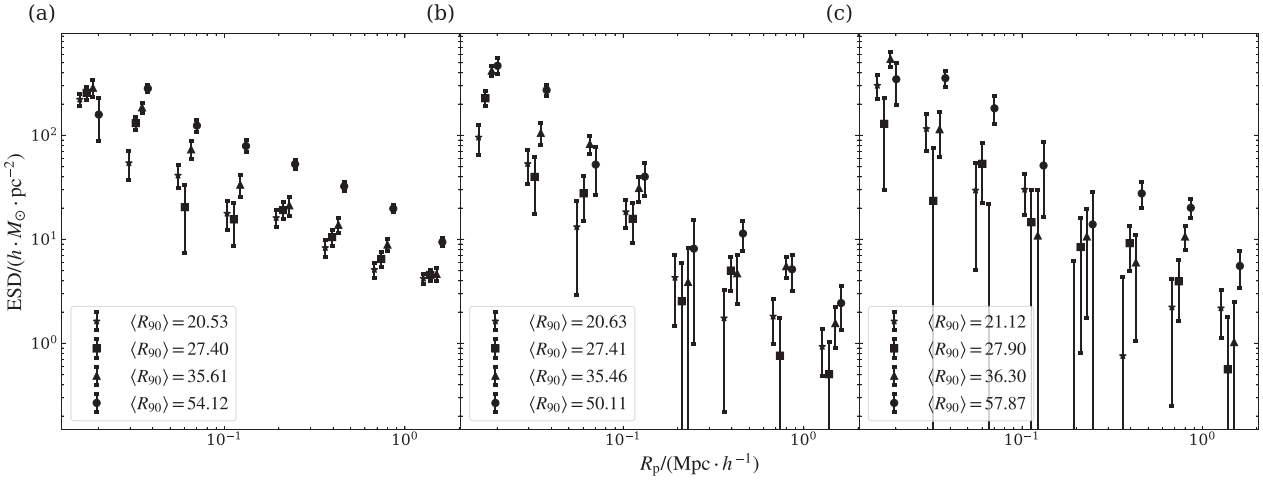

Fig. 4 (a) The ESD of red galaxy sub-samples. (b) The ESD of blue galaxy sub-samples. (c) The ESD of blue galaxy sub-samples after being weighted. We apply a different coefficient to each sample's $R_{\rm p}$ (projected radius) to improve the visibility of the data points.

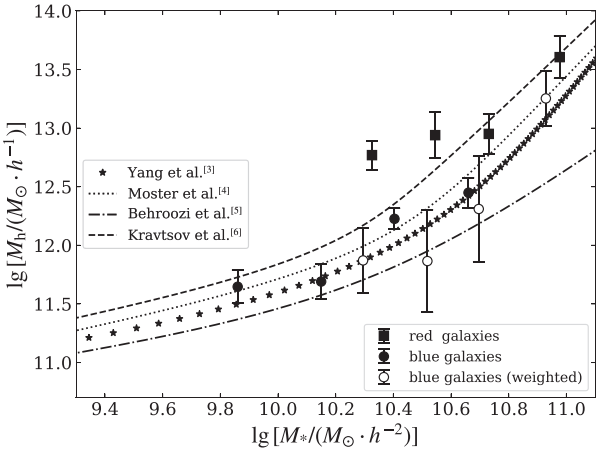

Fig. 5 The stellar-to-halo mass relation of red/blue galaxy sub-samples. The results for the sub-samples in Table 1 are represented by solid squares and solid circles, while the weighted blue galaxy sub-samples in Table 2 are represented by hollow circles.

5.2 Correlation between galaxy size and halo mass

The correlations between galaxy size and halo mass, stellar mass and galaxy size, $\lg(M_{\rm h}/M_*)$ (ratio of halo mass to stellar mass) and galaxy size of sub-samples in Tables 1 and 2 are all displayed in Fig. 6. Figure 6 (a) shows the correlation between galaxy size and halo mass in the sub-samples from Tables 1 and 2. It is clear that as the $\langle R_{90}\rangle$ increases, the halo mass in blue galaxy sub-samples also increases significantly. The red galaxy sub-samples show a similar trend. Fig. 6 (b) and Fig. 6 (c) show a significantly positive relationship between stellar mass and galaxy size ($\langle R_{90}\rangle$ and $\langle R_{50}\rangle$ (Petrosian radius, including 50% of the flux)). However, $\langle R_{50}\rangle$ has a more dispersed distribution, especially for the weighted sub-samples, which could introduce additional errors. Therefore, R_{90} is a more suitable parameter than R_{50} for investigating the correlation between galaxy size and halo mass.

Since there is a significantly positive stellar-to-halo mass relation, we calculate the ratio of halo mass to stellar mass, $\lg(M_{\rm h}/M_*)$, for the galaxy sub-samples in Tables 1 and 2 (see Fig. 6 (d)). It is clear that the $\lg(M_{\rm h}/M_*)$ does not increase with growing galaxy size. This indicates that the positive correlation between galaxy size and halo mass shown in Fig. 6 (a) is a spurious signal. The underlying reason is that as galaxy size increases, there is an accompanying increase in stellar mass, leading to higher halo mass.

Table 2 The parameters distribution of the blue galaxy sub-samples after being weighted based on the stellar mass-redshift distribution of the red galaxy sub-samples

Color	R_{90} /kpc	$\langle R_{90}\rangle$ /kpc	$\langle \lg M_*\rangle$ $/(M_\odot \cdot h^{-2})$	$\langle z\rangle$	$N_{\rm sub\text{-}sample}$
Blue	17 – 24	21.12	10.29	0.083	61325
	24 – 31	27.90	10.52	0.103	62805
	31 – 41	36.30	10.70	0.123	61196
	41 – 315	57.87	10.93	0.146	41452

In order to eliminate the effect of stellar mass on halo mass, we use the second red/blue galaxy sub-sample ($24 < R_{90} \leqslant 31$) as the reference and apply weights to the other red/blue galaxy sub-samples. Table 3 shows the detailed information of each weighted sub-sample. Fig. 7 and Fig. 8 show ESD and correlation between galaxy size and halo mass for each sub-sample in Table 3, respectively. After being weighted, the four sub-samples within red galaxies have the same stellar mass-redshift distribution, and the same for blue galaxies. We perform a linear fit to further quantify the correlation between galaxy size and halo mass:

$$M_{\rm h\_red} = -0.0023^{+0.0002}_{-0.0054}\langle R_{90}\rangle_{\rm red} + 13.0652^{+0.1756}_{-0.0054}\,, \tag{25}$$

$$M_{\rm h\_blue} = 0.0237^{+0.0004}_{-0.0108}\langle R_{90}\rangle_{\rm blue} + 11.2347^{+0.3106}_{-0.0108}\,. \tag{26}$$

The notation $M_{\rm h\_red}$ represents the halo mass of the red galaxy sub-sample, while $M_{\rm h\_blue}$ denotes the halo mass of the blue galaxy sub-sample. Similarly, $\langle R_{90}\rangle_{\rm red}$ and $\langle R_{90}\rangle_{\rm blue}$ refer to the $\langle R_{90}\rangle$ of

the red and blue galaxy sub-samples, respectively. The fitted slope for correlation between galaxy size and halo mass is close to zero in the red galaxy sub-samples, while the blue galaxy sub-samples show a slight deviation from zero.

However, the R_{90} difference between the first and last blue galaxy sub-samples is about 25 kpc, and the maximum change in halo mass caused by galaxy size is nearly equal to the error in halo mass. Considering the error, we conclude that there is no significant correlation between galaxy size and halo mass.

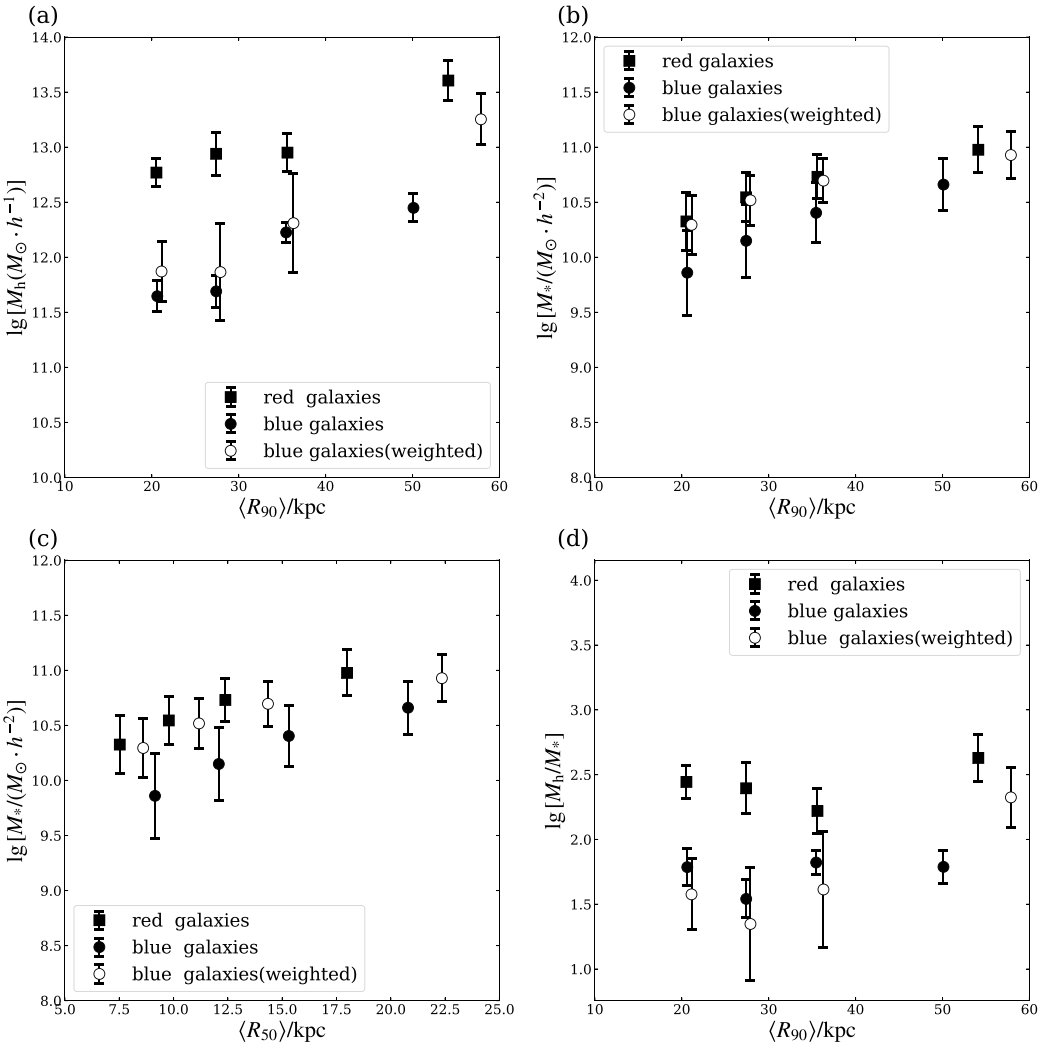

Fig. 6 (a) The correlation between galaxy size and halo mass for the sub-samples in Tables 1 and 2 is presented. The solid squares represent the correlation between galaxy size and halo mass for red galaxies, while the solid circles represent the correlation for blue galaxies. The hollow circles represent the results after adding weights. (b), (c) The relation between stellar mass and galaxy size ($\langle R_{90}\rangle$ and $\langle R_{50}\rangle$) in Table 1 and Table 2. (d) The correlation between $\lg(M_{\rm h}/M_*)$ and galaxy size for the galaxy sub-samples in Tables 1 and 2.

5.3 Correlation between galaxy color and halo mass

In Fig. 5 and Fig. 6 (a), we find that when the size, stellar mass, and redshift are similar, the halo mass differences between red and blue galaxies gradually vary with increasing stellar mass. This result is similar to that of Rodríguez-Puebla et al.[50]. Rodríguez-Puebla et al.[50] also pointed out that there are statistically significant differences in the average SHMR curves of their red and blue central galaxy sub-samples, which vary with halo mass. This suggests that the necessity of taking the difference in galaxy color into account when studying the correlation between galaxy properties and halo mass.

5.4 Hydrodynamical simulation

Here, we use the cosmological hydrodynamical simulation program Illustris-TNG50 (The Next Generation Illustris project)[51–52] to investigate the correlation between half-mass radius ($R_{1/2}$, comoving scale) and halo mass at redshift 0.1. The constraints of the Illustris-TNG50 theoretical model on galaxies with very small/large radii are poor, so we have discarded data points in this range which have significant errors. The correlations between halo mass and $R_{1/2}$, as well as $\lg(M_{\rm h}/M_*)$ and $R_{1/2}$, are displayed in Fig. 9. The correlation between halo mass and $R_{1/2}$ appears to be positively correlated in Fig. 9 (a), but $\lg(M_{\rm h}/M_*)$ remains constant as $R_{1/2}$ changes in Fig. 9 (b). This indicates that the signal in Fig. 9 (a) is a spurious signal, and the change in halo mass is mainly caused by stellar mass, which is consistent with our previous results.

Table 3 The parameters distribution of each sub-sample after adding weights based on the stellar mass-redshift distribution of the second sub-sample ($24 < R_{90} \leqslant 31$) of both the red and blue galaxies as the reference

Color	R_{90} /kpc	$\langle R_{90}\rangle$ /kpc	$\langle \lg M_*\rangle$ $/(M_\odot \cdot h^{-2})$	$\langle z\rangle$	$N_{\rm sub\text{-}sample}$
Red	17 – 24	21.16	10.52	0.102	74765
	24 – 31	27.40	10.55	0.103	69791
	31 – 41	34.91	10.55	0.103	73459
	41 – 315	47.71	10.53	0.103	75098
Blue	17 – 24	21.03	10.14	0.095	61325
	24 – 31	27.41	10.15	0.095	62805
	31 – 41	34.73	10.15	0.095	61196
	41 – 315	46.35	9.99	0.094	41452

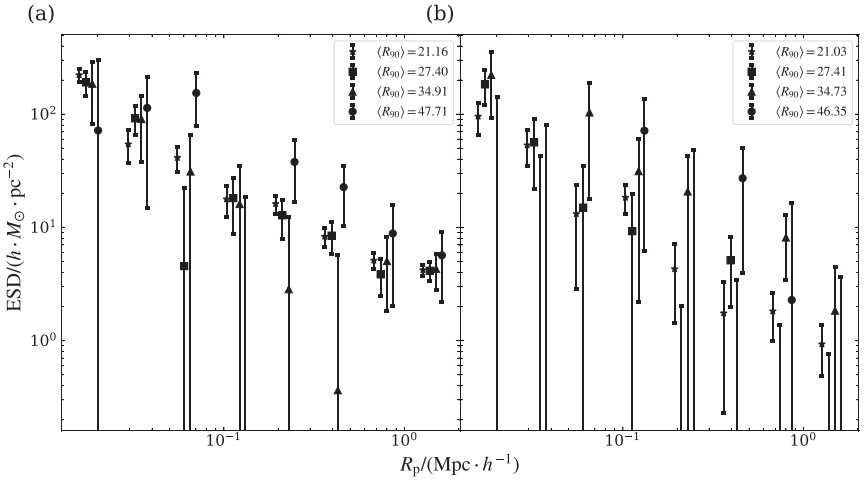

Fig. 7 The ESD for each galaxy sub-sample in Table 3 is shown. (a) The ESD of the red galaxy sub-samples. (b) The ESD of the blue galaxy sub-samples. We apply a different coefficient to the $R_{\rm p}$ of each sub-sample to improve the visibility of the data points.

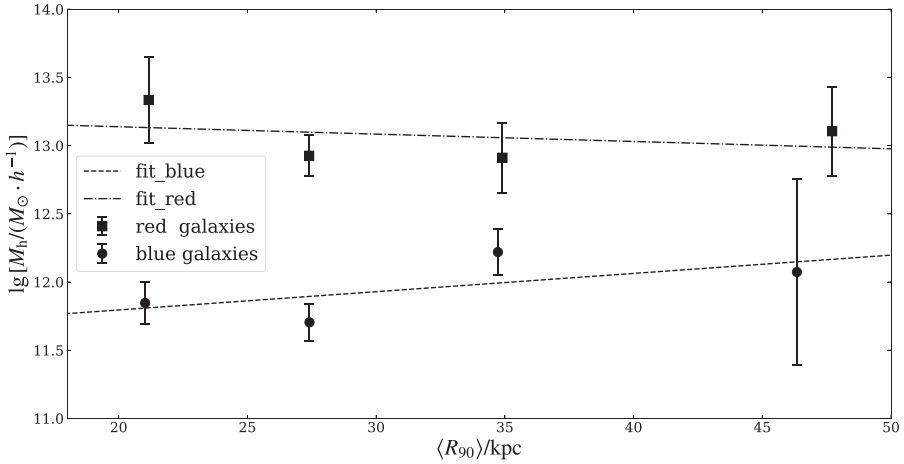

Fig. 8 The correlation between galaxy size and halo mass in the red and blue galaxy sub-samples of Table 3. The dash-dotted line and dashed line represent the fitted linear relationships between galaxy size and halo mass for the sub-samples of red and blue galaxies, respectively.

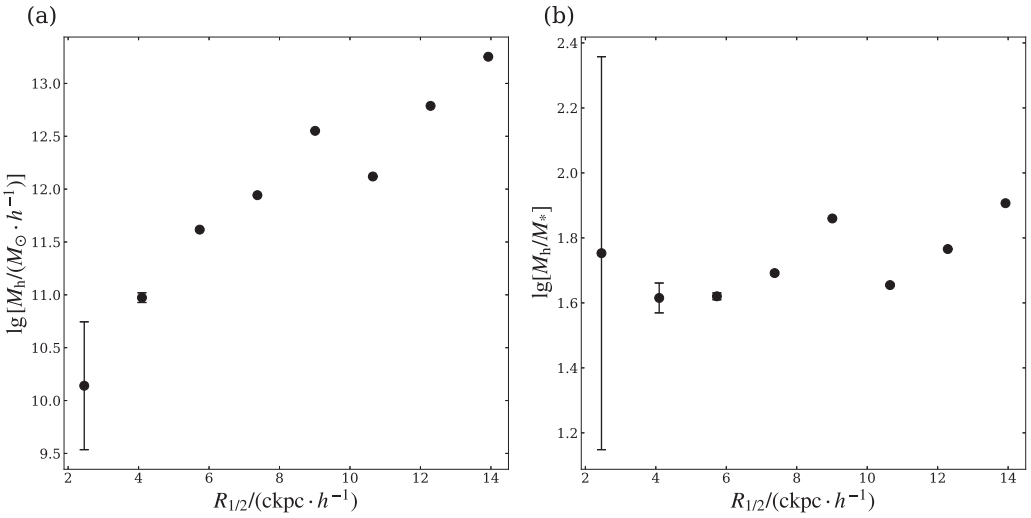

Fig. 9 (a) Results from the Illustris-TNG50 simulation on the correlation between stellar half-mass radius ($R_{1/2}$) and halo mass. ckpc is comoving kiloparsecs. (b) The relation between $\lg(M_{\rm h}/M_*)$ and $R_{1/2}$ in the Illustris-TNG50 simulation is shown.

6 Discussion

The main result of our work is that there is no significant correlation between galaxy size and halo mass within the redshift range of $0.02 \leqslant z \leqslant 0.2$ and stellar mass range of $8 \leqslant \lg[M_*/(M_\odot \cdot h^{-2})] \leqslant 12$. The primary result of our study is obtained from measurements of observational data using the galaxy-galaxy lensing method and is supported by the results of the Illustris-TNG50 hydrodynamical simulations. There are two advantages of measuring directly with observational data instead of relying on hydrodynamical simulations for research: first, the results from observational data can avoid many assumptions, and

there is no newly introduced systematic error; second, the abundance matching mechanism commonly used in hydrodynamical simulations is still developing, and the simulation cannot fully reproduce the galaxy structure we observed today in universe[53–54]. These indicate the existence of certain limitations in hydrodynamic simulations compared to observational data. To mitigate these limitations, we use Illustris-TNG50 instead of Illustris-TNG300. Illustris-TNG50 has a higher temporal and spatial resolution, which more suitable for studying galaxy evolution issues.

Figure 5 shows that for the same stellar mass, the mass of halo resided by red galaxy is usually larger than that of blue galaxy. Wang et al.[55] indirectly measured the halo mass by examining the number of satellite galaxies near central galaxies. They found that for same stellar masses greater than $10^{11.2}M_{\odot}$, red central galaxies have about twice as many satellite galaxies as blue central galaxies. Similar conclusions were drawn by Mandelbaum et al.[37] in their study of red and blue central galaxy samples, and they suggested that this may be due to some certain underlying physical processes. Fig. 6 and Fig. 9 suggest that the increase in halo mass is due to rising in stellar mass, rather than galaxy size.

Figure 8 shows our main results: the linear regression slope between red galaxy size and halo mass is $-0.0023^{+0.0002}_{-0.0054}$, while for blue galaxies, it is $0.0237^{+0.0004}_{-0.0108}$. Considering the presence of measurement errors, we conclude that there is no significant correlation between galaxy size and halo mass in redshift range of $0.02 \leqslant z \leqslant 0.2$ and stellar mass range of $8 \leqslant \lg[M_*/(M_{\odot} \cdot h^{-2})] \leqslant 12$. This result is consistent with many previous studies[14–18, 20].

Shankar et al.[14] analyzed several semi-analytical models and found that most of them predict a positive correlation between galaxy size and halo mass at fixed stellar mass. Shankar et al.[14] showed that this correlation can arise simply as the result of dissipationless mergers. For a given increase in stellar mass, minor mergers produce a higher increase in galaxy size than major mergers[56–57]: if minor mergers are more frequent in more massive halos, this can lead to a significant correlation between galaxy size and halo mass even when the stellar mass is constant. In addition, if the stellar mass is fixed, factors such as the instability of disks, gas dissipation in major mergers, and differences in the accretion of galaxies in low-mass and high-mass halos may also lead to a positive correlation between galaxy size and halo mass. Shankar et al.[14] discuss these mechanisms in detail and point out that existing observational data do not support the correlation between galaxy size and halo mass in these models[58]. Meanwhile, there is little observational evidence for a correlation between circular velocity (a proxy for halo mass) and disc size for isolated disc galaxies[8, 59].

Our results slightly differ from Charlton et al.[8]. They utilized the galaxy-galaxy lensing technique to measure the correlation between galaxy half-light radius and halo mass. After binning in luminosity and galaxy half-light radius, they studied the variation in halo mass, taking into account the dependence of halo mass on stellar mass. They constructed a functional form, which is given by

$$M_{\rm h}(M_*) \propto r^{\beta}_{\rm eff}(M_*)\,. \tag{27}$$

The parameter β serves as a fitting coefficient, quantifying the correlation between galaxy size and halo mass, while $r_{\rm eff}(M_*)$ is half-light radius. The final measured value of β is 0.42 ± 0.16. This indicates a positive correlation between galaxy size and halo mass. The Eq. (27) proposed by Charlton et al.[8] expresses halo mass as a function of stellar mass, and this function is based on the SHMR curve fitted by Moster et al.[4] (see Fig. 5). This

means that the accuracy of their results depends on a precise description of SHMR. However, there is a significant dispersion of up to 1 dex in halo mass for the same stellar mass within the previous SHMR curves. This discrepancy could lead to significant differences between Charlton et al.'s results and the actual state of affairs[8].

Sonnenfeld et al.[19, 60] found that their results also support a positive correlation between galaxy size and halo mass when stellar mass measurement errors are ignored, with a correlation strength similar to Charlton et al.[8].

In contrast, our approach of weighting the galaxy sub-samples does not rely on previously fitted SHMR or other models. In Fig. 8, the measurement errors in the halo mass for the well-fitted galaxy sub-samples are less than 0.2 dex, while for others, the errors are less than 0.7 dex. Compared to previous studies, our results show slightly larger errors for those poorly fitted sub-samples. This discrepancy is mainly due to the limited number of galaxies with small or large radii in the observational data. Weighting the sub-samples requires a sufficiently large galaxy sample within a specific range of stellar mass and redshift. Achieving identical distributions of stellar mass and redshift for each sub-sample is challenging when the galaxy count is low (as shown in Table 1, where there are slight variations in the average stellar mass of the sub-samples), which affects the ESD and halo mass measurements for these galaxy sub-samples. In the future, with an increase in observational data, a larger sample of galaxies will significantly improve the precision of our method.

Merger events play an important role in galaxy size and stellar mass growth. Minor mergers are generally thought to result in a greater increase in galaxy size than major mergers when it comes to the growth of galaxies with the same stellar mass. If there is no correlation between galaxy size and halo mass, then the timescale for galaxy mergers in high-mass halos and the rate of minor mergers should be similar to those in low-mass halos. This means that models suggesting faster size growth for galaxies in high-mass halos compared to low-mass halos may not be consistent with the observational data. Considering the lack of correlation between galaxy size and halo mass, the dispersion (about 0.2 dex) in the relation between stellar mass and halo mass is not due to galaxy size. Intuitively, one might expect that a halo with a more concentrated mass distribution could lead to galaxies with more concentrated mass distribution. Thus, this dispersion could be more closely related to the concentration parameter or the spin of the halo[8, 61].

7 Summary and conclusions

Modern galaxy formation theory suggests that halo mass plays a crucial role in the galaxy formation process. As a result, the correlation between observable galaxy properties (such as stellar mass, size, and spin) and halo mass has been a topic of great significance in the field. In this thesis, we focus on studying the correlation between galaxy size and halo mass by analyzing data from the Sloan Digital Sky Survey DR7. We classify the lens galaxy sample into red and blue galaxy samples and further divide them into eight sub-samples based on galaxy size. The redshift, stellar mass, and R_{90} ranges of galaxy sub-samples are $0.02 \leqslant z \leqslant 0.2$, $8 \leqslant \lg[M_*/(M_\odot \cdot h^{-2})] \leqslant 12$, and $R_{90} > 17$ kpc, respectively. We use two methods to mitigate the impact of stellar mass on the correlation between galaxy size and halo mass: introducing a new variable $\lg(M_{\rm h}/M_*)$, or weighting the sub-samples. Finally, our main results can be summarized as follows:

I. We perform a linear regression analysis to

determine the correlation between galaxy size and halo mass with fixed stellar mass and redshift. The fitted slope of red galaxies is $-0.0023^{+0.0002}_{-0.0054}$ and blue galaxies $0.0237^{+0.0004}_{-0.0108}$. Considering measurement errors, we conclude that there is no significant correlation between galaxy size and halo mass. This suggests that the dispersion (0.2 dex) of stellar-to-halo mass relation is not due to galaxy size. Our results indicate that the growth rate of galaxy size and the rate of minor mergers are unrelated with halo mass.

II. Our study suggests that the increasing halo mass may not be the cause of galaxy size increase, which seems inconsistent with the appearance of simultaneous increase in these two indexes. On the contrary, stellar mass is more likely influenced by halo mass. To better understand the correlation between galaxy size and halo mass, we need to further reduce the influence of other galaxy properties on the correlation between galaxy size and halo mass.

III. We find that the mass of halo resided by red galaxy is usually larger than that of blue galaxy with same stellar mass. This may be attributed to the fact that the increase in stellar mass of red galaxies more significantly depends on mergers, while the growth of stellar mass in blue galaxies is more reliant on the star formation process. And the halo mass differences between red and blue galaxies gradually vary with increasing stellar mass. It suggests that the necessity of taking the difference in galaxy color into account when studying the correlation between galaxy properties and halo mass.

Weighting the galaxy samples is an effective method which allows us to control certain variables in our study. We can use this method to study the correlation between other galaxy properties (such as Sérsic index and spin) and halo mass in coming years. However, this method requires a sufficient number of galaxies. In the future, as more observational data of galaxies become available, the stellar mass redshift distribution can be classified into more bins to improve the measurement accuracy. The constraints of the Illustris-TNG50 theoretical model on galaxies with very small/large radii are poor, requiring the development of more appropriate galaxy evolution models to reproduce a more real galaxy formation process.

Acknowledgements We thank Qinxun Li, Wei Liu, and Ziwen Zhang for helpful discussions.

Reference

[1] Faber S M, Gallagher J S. ARA&A, 1979, 17: 135
[2] Conroy C, Wechsler R H, Kravtsov A V. ApJ, 2006, 647: 201
[3] Yang X, Mo H J, Van den Bosch F C. ApJ, 2009, 695: 900
[4] Moster B P, Somerville R S, Maulbetsch C, et al. ApJ, 2010, 710: 903
[5] Behroozi P, Wechsler R H, Hearin A P, et al. MNRAS, 2019, 488: 3143
[6] Kravtsov A V, Vikhlinin A A, Meshcheryakov A V. AstL, 2018, 44: 8
[7] Leauthaud A, Tinker J, Bundy K, et al. ApJ, 2011, 744: 159
[8] Charlton P J L, Hudson M J, Balogh M L, et al. MNRAS, 2017, 472: 2367
[9] Vale A, Ostriker J. MNRAS, 2006, 371: 1173
[10] Zu Y, Mandelbaum R. MNRAS, 2015, 454: 1161
[11] Cooper M C, Griffith R L, Newman J A, et al. MNRAS, 2012, 419: 3018
[12] Yoon Y, Im M, Kim J W. ApJ, 2017, 834: 73
[13] Huang S, Leauthaud A, Greene J, et al. MNRAS, 2018, 480: 521
[14] Shankar F, Mei S, Moreno J, et al. MNRAS, 2014, 439: 3189
[15] Newman A B, Ellis R S, Andreon S, et al. ApJ, 2014, 788: 5
[16] Allen R J, Kacprzak G G, Spitler L R, et al. ApJ, 2015, 806: 3

[17] Damjanov I, Zahid H J, Geller M J, et al. ApJ, 2015, 815: 104
[18] Saracco P, Gargiulo A, Ciocca F, et al. A&AC, 2017, 597: A122
[19] Sonnenfeld A, Wang W, Bahcall N. A&AC, 2019, 622: A30
[20] Sonnenfeld A, Tortora C, Hoekstra H, et al. A&AC, 2022, 662: A55
[21] Desmond H. MNRAS, 2016, 464: 4160
[22] Desmond H. MNRAS, 2017, 472: L35
[23] Desmond H, Katz H, Lelli F, et al. MNRAS, 2019, 484: 239
[24] Taylor E N, Cluver M E, Duffy A, et al. MNRAS, 2020, 499: 2896
[25] Erben T, Hildebrandt H, Miller L, et al. MNRAS, 2013, 433: 2545
[26] Aihara H, Arimoto N, Armstrong R, et al. PASJ, 2018, 70: S4
[27] Mandelbaum R, Miyatake H, Hamana T, et al. PASJ, 2018, 70: S25
[28] de Jong J T A, Verdoes Kleijn G A, Kuijken K H, et al. ExA, 2013, 35: 25
[29] Luo W, Silverman J D, More S, et al. arXiv: 220403817
[30] Luo W, Yang X, Zhang J, et al. ApJ, 2017, 836: 38
[31] Mandelbaum R, Tasitsiomi A, Seljak U, et al. MNRAS, 2005, 362: 1451
[32] Lupton R, Gunn J E, Ivezi Z, et al. adass, 2001, 238: 269
[33] Bernstein G M, Jarvis M. ApJ, 2002, 123: 583
[34] Yang X, Mo H J, Van den Bosch F C, et al. ApJ, 2007, 671: 153
[35] Blanton M R, Schlegel D J, Strauss M A, et al. ApJ, 2005, 129: 2562
[36] Baldry I K, Glazebrook K, Brinkmann J, et al. ApJ, 2004, 600: 681
[37] Mandelbaum R, Wang W, Zu Y, et al. MNRAS, 2016, 457: 3200
[38] Yang X H, Mo H, van den Bosch F C. ApJ, 2008, 676: 248
[39] Miyatake H, Battaglia N, Hilton M, et al. ApJ, 2019, 875: 63
[40] Yang X, Mo H J, Van Den Bosch F C, et al. MNRAS, 2006, 373: 1159
[41] Mandelbaum R, Li C, Kauffmann G, et al. MNRAS, 2009, 393: 377
[42] Navarro J F, Frenk C S, White S D M. ApJ, 1997, 490: 493
[43] Leauthaud A J, Benson A, Civano F, et al. MNRAS, 2015, 446: 1874
[44] Guzik J, Seljak U. MNRAS, 2002, 335: 311
[45] Tinker J L, Weinberg D H, Zheng Z, et al. ApJ, 2005, 631: 41
[46] Lewis A. PhRvD, 2013, 87: 103529
[47] Tinker J L, Robertson B E, Kravtsov A V, et al. ApJ, 2010, 724: 878
[48] Goodman J, Weare J. CAMCoS, 2010, 5: 65
[49] Bilicki M, Dvornik A, Hoekstra H, et al. A&AC, 2021, 653: A82
[50] Rodríguez-Puebla A, Avila-Reese V, Yang X, et al. ApJ, 2015, 799: 130
[51] Pillepich A, Nelson D, Springel V, et al. MNRAS, 2019, 490: 3196
[52] Nelson D, Pillepich A, Springel V, et al. MNRAS, 2019, 490: 3234
[53] Rodriguez-Gomez V, Snyder G F, Lotz J M, et al. MNRAS, 2019, 483: 4140
[54] Zanisi L, Huertas-Company M, Lanusse F, et al. MNRAS, 2021, 501: 4359
[55] Wang W, White S D M. MNRAS, 2012, 424: 2574
[56] Naab T, Johansson P H, Ostriker J P. ApJ, 2009, 699: L178
[57] Hopkins P F, Hernquist L. MNRAS, 2010, 407: 447
[58] Shankar F, Mei S, Bernardi M, et al. ApJ, 2013, 779: 29
[59] Lelli F, McGaugh S S, Schombert J M. ApJ, 2016, 152: 157
[60] Sonnenfeld A, Leauthaud A. MNRAS, 2018, 477: 5460
[61] Wechsler R H, Tinker J L. ARA&A, 2018, 56: 435

星系-星系透镜效应下星系大小与晕质量的相关性

闫大伟[1,2] 王晴晴[1,2] 张聪聪[1,2] 罗文涛[1,2] 方文娟[1,2] 张育飞[3]
李佳迅[1,2]

(1 中国科学技术大学物理学院天文系 合肥 230026)
(2 中国科学技术大学天文与空间科学学院 南京 210023)
(3 乐山师范学院数理学院 乐山 614000)

摘要 星系-星系透镜技术可用于研究星系大小与晕质量的相关性. 按照星系大小、恒星质量和颜色将来自斯隆数字巡天第7次发布的数据(SDSS DR7)中的星系群样本的星系样本分为不同的子样本. 通过对每个星系子样本的面密度超出进行建模以获得其晕质量. 没有在红/蓝星系大小与晕质量之间观察到强相关性. 红/蓝星系大小与晕质量关系的拟合斜率分别为$-0.0023^{+0.0002}_{-0.0054}$和$0.0237^{+0.0004}_{-0.0108}$. 通过使用Illustris-TNG (下一代Illustris项目)数据集提供的半质量半径, 可以将观测的结果与Illustris-TNG的模拟结果进行比较. 与观测不同的是, Illustris-TNG模拟的晕质量呈现出增加的趋势, 这主要是由于恒星质量与星系大小之间存在正相关性. 当晕质量除以恒星质量时, 这种依赖性消失了, 表明Illustris-TNG的模拟结果与观测的结果相似.

关键词 引力透镜: 弱, 星系: 晕, 星系: 基本参数, 方法: 数据分析